AGU PUBLICATIONS

Geophysical Research Letters

RESEARCH LETTER
10.1002/2013GL058935

Key Points:
- M_w 8.1 2004 Macquarie event triggers secondary event
- Separation of high-frequency and low-frequency radiation
- Energy projection without use of large arrays

Supporting Information:
- Readme
- Supplmat.pdf

Correspondence to:
B. L. N. Kennett,
Brian.Kennett@anu.edu.au

Citation:
Kennett, B. L. N., A. Gorbatov, and S. Spiliopoulos (2014), Tracking high-frequency seismic source evolution: 2004 M_w 8.1 Macquarie event, *Geophys. Res. Lett.*, *41*, 1187–1193, doi:10.1002/2013GL058935.

Received 2 DEC 2013
Accepted 15 JAN 2014
Accepted article online 17 JAN 2014
Published online 22 FEB 2014

Tracking high-frequency seismic source evolution: 2004 M_w 8.1 Macquarie event

B. L. N. Kennett[1], A. Gorbatov[2], and S. Spiliopoulos[2]

[1]Research School of Earth Sciences, Australian National University, Canberra, ACT, Australia, [2]Geoscience Australia, Canberra, ACT, Australia

Abstract The 2004 M_w 8.1 event on 23 December 2004 near the Macquarie Ridge is a very large intraplate event that has been overshadowed by the M_w 9.3 Sumatra-Andaman event only 3 days later. We are able to track the progress of source evolution by estimating the progression of the points of energy emission, exploiting the good azimuthal distribution of available stations. The results indicate that this event ruptured on two nearby fault systems reactivating fossil fracture zones, with the second subevent to the west triggered by the first. The total duration of high-frequency radiation is quite short, about 60 s, for such a large event. Much of the high-frequency radiation occurs on a fault subparallel to that inferred from long-period studies. This composite fault behavior with displaced triggered failure appears to be a characteristic of large intraplate events beneath the oceans.

1. Introduction

There has been considerable success in evaluating the behavior of great earthquakes using backprojection from dense arrays. The initial effort by *Ishii et al.* [2005] for the great Sumatra-Andaman event using the Hi-net array in Japan was followed by exploitation of global stations by *Walker et al.* [2005] and *Walker and Shearer* [2009]. Most studies, however, have concentrated on localized arrays, with extensive use of the Japanese Networks [e.g., *Wang and Mori*, 2011], as well as the USArray and European stations used as an array [e.g., *Simons et al.*, 2011].

However, some significant events do not lie at a convenient distance from such arrays. The M_w 8.1 event north of Macquarie Island at 14:59 on 23 December 2004 was almost immediately overshadowed by the M_w 9.3 Sumatra-Andaman event on 26 December with its associated devastating tsunami. Further, this event is beyond 90° epicentral distance for much of Japan and all European and North American stations, and so is not at all suited to conventional backprojection methods.

We demonstrate that effective results for the source evolution can be obtained by using a broad azimuthal distribution of stations, building on the well-developed criteria for hypocenter determination. We concentrate on the estimation of the location of energy emission as a function of time (the *evocenter*) by using energy stacks across a grid that expands away from the hypocenter.

2. Tracking High-Frequency Source Evolution

The hypocenter, the point of initiation of seismic energy, is determined by exploiting the arrival times of recognized seismic phases across a broad group of seismic stations. It is well recognized that a good azimuthal distribution of stations is needed to get tight control on the hypocenter and that only weak control is achievable when the event lies well outside the available network of stations [e.g., *Engdahl et al.*, 1998; *Bondar and Storchak*, 2011].

Our approach to following the evolution of a seismic source is based on extending the idea of tracking energy emission to subsequent times, making use of the energy on the seismic traces as a function of time. We exploit the time residuals from the hypocenter determination to correct for the influence of 3-D structure and then work with a 1-D reference model, e.g., ak135 [*Kennett et al.*, 1995], to construct the times of passage for relevant seismic phases from points in the neighborhood of the hypocenter to the various seismic stations. We fix the initial point at the hypocenter and then allow the search region to grow, commonly with the local *P* wave velocity. This still keeps the domain a reasonable size but should allow for any style of rupture in a single event.

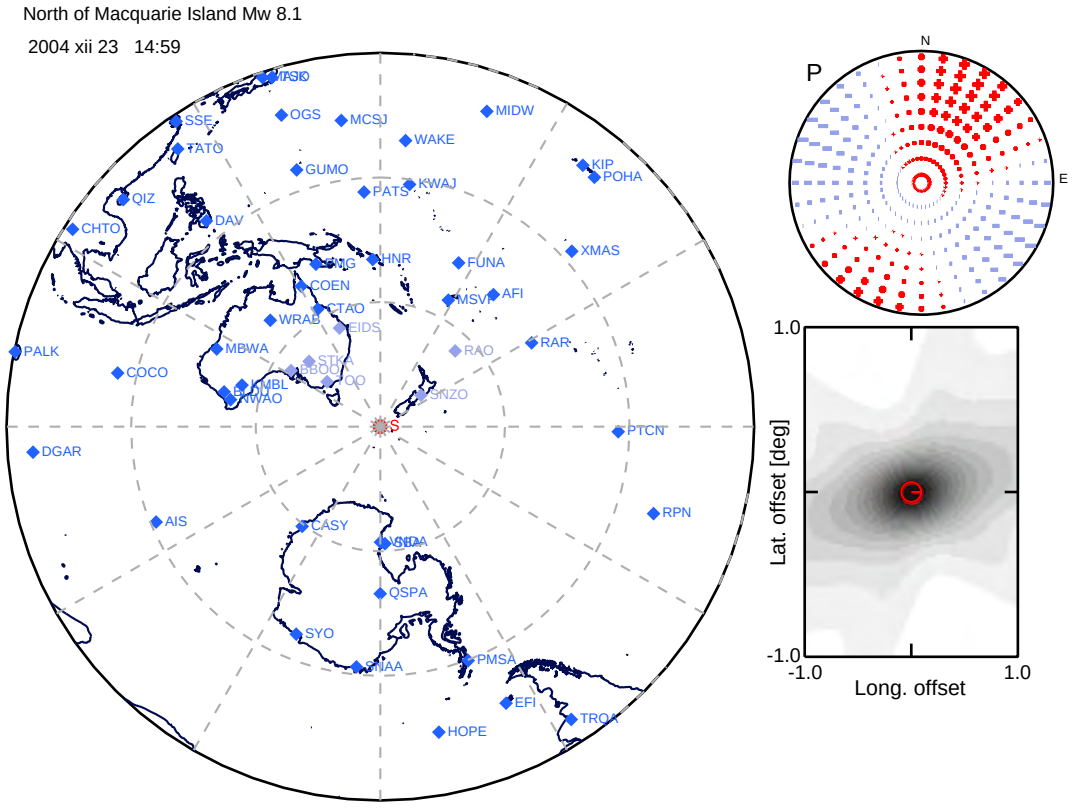

Figure 1. The configuration of the available broadband stations for the 2004 Macquarie Islands M_w 8.1 event and the resulting spatial resolution available at the hypocenter, together with the *P* wave radiation for the global centroid moment tensor solution. Stations within 30° epicentral distance are indicated in lighter tone. The spatial resolution diagram for energy summation is constructed by superposition of Gaussian profiles about the isochron for *P* arrivals from the target point indicated by the red symbol, with width modulated by the inverse slowness for *P*. The energy resolution function is contoured with 16 equal gray increments so that the 3 dB level is approximately 25 km in the EW direction and somewhat less in the NS direction.

What we seek to achieve is to map the energy contained in time segments of the seismograms to their point of emission. We can judge the capacity for spatial localization by summing the energy contributions around the reciprocal isochrons that pass through a target location tracked from each of the stations. To map from time into space from station *j*, a time interval τ is modulated by the inverse spherical slowness $\wp_j$. We can approximate the effects of finite frequency by employing a Gaussian profile with a half width of $1/f_p\wp_j$ for peak frequency f_p

In Figure 1 we display the available broadband station configuration within 90° of the 2004 Macquarie Island event and the estimated spatial operator for the energy stack using these stations, using a conservative value of 1 Hz for peak frequency. We see that by using the full azimuthal distribution of stations, we are able to achieve a spatial operator with a rapid fall off from a strong central peak, no more than 25 km across at the 3 dB level. At 2 Hz the theoretical resolution is comparable to the accuracy achievable in hypocenter determination. The spatial resolution pattern in Figure 1 broadens only slightly if the few stations closer than 30° are excluded.

Figure 1 has been constructed using equal weight for all stations, but even downgrading oceanic stations because of their commonly poorer signal-to-noise ratio does not make much difference to the achievable spatial resolution. Because we have the potential for such effective spatial resolution, we can now test putative locations of energy emission and select the one with the highest energy stack. Resolution in depth can be estimated in a similar way and is again around 20 km, which is not really adequate to delineate the behavior in depth.

For a sequence of time intervals of length δt after the origin time of the earthquake we construct a measure of the energy emission associated with any spatial location as

$$\mathcal{E}_k(T) = \sum_j \int_0^{\delta t} \mathrm{d}\tau\, w(\tau) u_j^2(T + t_{jk} + \tau), \tag{1}$$

where t_{jk} is the travel time for a phase to the station set $\{\mathbf{x}_j\}$, u_j the corresponding seismogram, and we employ a window function $w(t)$. We can also include trace normalization and weighting by signal-to-noise ratio in the estimator $\mathcal{E}$. The best estimate of the location of energy emission, for the stations employed, is then extracted as

$$\mathbf{x}_e(t_0 + T) = \mathbf{x}(\max_k \mathcal{E}_k(T)). \tag{2}$$

The offset time T is initially set as 0 and then progressively incremented by δt with a sequence of evocenters estimated to chart the progress of the energy emission by the seismic source. For further discussion of the technique and its relation to other methods, see the supporting information.

3. The 2004 M_w 8.1 Macquarie Event

The 23 December 2004 earthquake occurred about 150 km off the main plate boundary on the oceanic crust of the Australian Plate in a region that has undergone complex deformation in the last 25 Myr [e.g., *Mosher and Massell Symons*, 2008; *Hayes et al.*, 2009] and sits in the transition from oblique subduction at the Puysegur Trough to strike slip, with some compression, on the Macquarie Ridge (Figure 2).

The Macquarie Block was originally the site of seafloor spreading with short ridge segments separated by multiple transform faults. Subsequent shifts in the pole of motion between the Australian and Pacific Plates have transformed the nature of the boundary, with strike-slip motion along the Macquarie Ridge leading into the Puysegur trench where the Australian Plate is subducting obliquely. The current convergence rate is about 30 mm/yr. The complex of conjugate transform faults associated with the former spreading have been extensively deformed with strong shearing in the last 20 Ma. The area is marked by ongoing seismicity, mostly along the ridge but also with splays to the former fracture zones [*Ruff et al.*, 1989].

In the last 40 years there have been two great earthquakes related to the Macquarie Ridge complex. The M_w 8.0 event on 23 May 1989 occurred on the ridge at 52.5°S with aftershocks on the relict fracture zones [*Das*, 1993]. The M_w 8.1 event on 23 December 2004 lies west of the Macquarie Ridge on the Australian Plate. A historic earthquake on 26 June 1924 is estimated to be at least M_w 7.8 and lies in a similar configuration to that in 2004 but a little farther west. In contrast, the Pacific Plate on the other side of the ridge shows little seismicity.

The standard Earth models used for teleseismic location are oriented toward subduction zone sources recorded at continental stations. Further, there are few close stations to provide any tight control, so absolute locations are less well determined than in other environments. Despite the overlap with the strong aftershock sequence from the 26 December 2004 M_w 9.1 Sumatra-Andaman event, *Robinson* [2011] successfully carried out a relative relocation of the larger aftershocks of the 23 December 2004 Macquarie event, which he terms the Tasman Sea event. The main pattern is a roughly linear feature with a strike of about 170° extending about 150 km either side of the hypocenter. A number of the aftershocks relocate to the west of the main cluster, close to neighboring fracture zones and the estimated location of the 1924 event.

Hayes et al. [2009] and *Robinson* [2011] present analyses of the long-period characteristics of the 23 December 2004 event. *Hayes et al.* [2009] present evidence for little directivity in source response and infer a source duration of around 100 s. *Robinson* [2011] points out that the dip and rake of the fault slip are poorly determined, even though the possible strike directions are much better constrained. The centroid depth could be quite deep (> 25 km), suggesting that much of the rupture occurs in the oceanic mantle [cf. *Abercrombie and Ekström*, 2001]. The preferred model of *Robinson* [2011], from body wave analysis, combines northern faulting with a strike of 160° and southern faulting with a strike of 178°. The two faults approximate the shape of the curved fracture zone 5 [*Mosher and Massell Symons*, 2008]. About 76% of the moment release occurs on the northern segment.

Our analysis of the 2004 December 23 event is based on the high-frequency radiation. We have used a band-pass filter with corners at 0.8 and 4.0 Hz and conducted energy stacks for 4 s windows advanced by

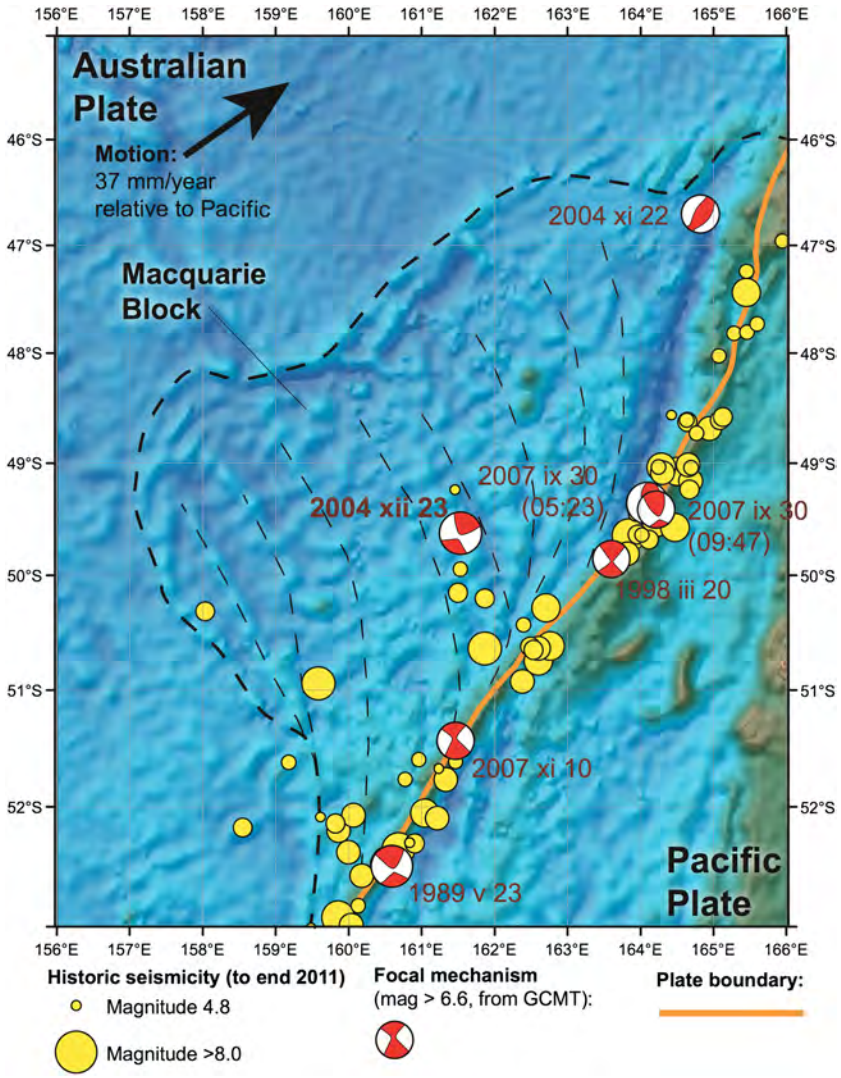

Figure 2. The location of events near the Macquarie Ridge, with moment tensors for events with M_w >6.6 indicating the complex tectonic configuration. The Macquarie Block is outlined, which may act as a microplate.

2 s steps. The travel time residuals for the *P* phases for this event show large residuals and strong directivity. Paths to Antarctic stations are fast, but those to stations in the northern Pacific are somewhat slow. We have therefore applied the time residuals with reversed sign to align the beginning of the energy emission to the hypocenter. We have then used the ak135 model [*Kennett et al.*, 1995] to determine the segments from the seismograms, at each station, to be used for stacking for the various test points on our grid. The spatial resolution pattern for the epicentral location shown in Figure 1 indicates potential resolution of about 15 km in the north-south direction and about 20 km in the east-west direction.

In Figure 3 we show our estimate of the locations of emission of high-frequency energy as a function of time after the initiation of the earthquake. Our search grid starts from the hypocenter and expands spatially at a velocity of 3.5 km/s, since there is no indication of supershear rupture. We employ a 3-D grid extending 10 km above and below the hypocenter. We present the results in plan view because we unfortunately have little discrimination in depth. On Figure 3 we display the nodal planes estimated from the centroid moment tensor, together with the main plate boundary and the approximate locations of the relict transform faults, which have limited ship track control. Given the potential error in location in this oceanic environment, it is indeed likely that the 2004 epicenter should lie on the fracture zone FZ5 (Figure 3) rather than displaced to

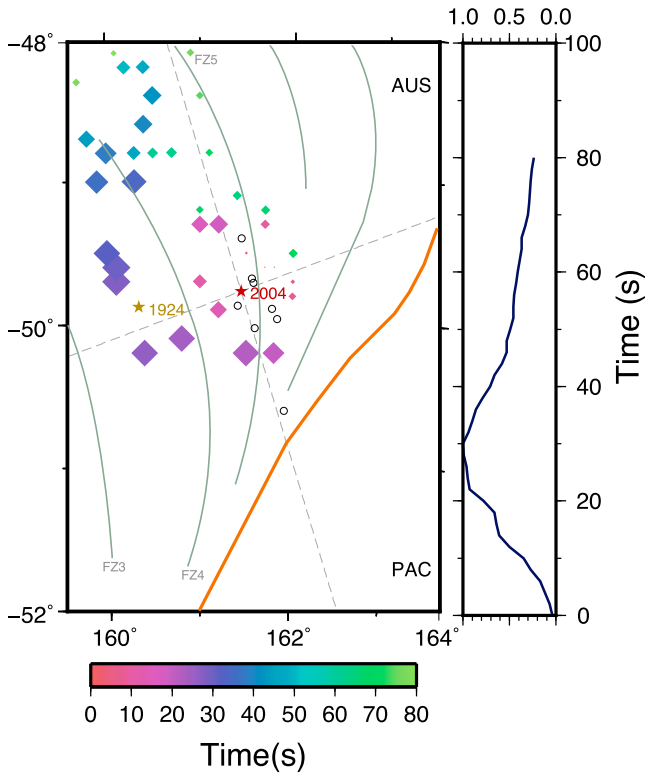

Figure 3. The progressive locations of the point of maximum high-frequency energy emission estimated from the full set of stations, using a grid expansion rate of 3.5 km/s from the hypocenter shown as a red star. The size of the symbols represents the level of the energy stack associated with successive time intervals. The symbols are scaled so that the largest is approximately the size of the 3 dB patch in the estimated spatial resolution for energy. The time profile of the high-frequency energy for the event is shown at the right. The teleseismically registered aftershocks are shown as open circles, and the estimated epicenter of the 1924 event is indicated by an orange star. We also display the fault planes extracted from the centroid moment tensor solution. The main plate boundary is shown in brown, and the approximate positions of the relict transform faults are plotted in gray.

the west. Such a displacement would bring the whole energy release pattern in closer concordance with the configuration of the fracture zones.

The initial phase of high-frequency energy emission steps to the north and then there appears to be more complex behavior with simultaneous energy release to the south of the epicenter, consistent with bilateral rupture. About 30 s after event initiation, at the peak of the high-frequency energy release, the evocenters transfer to a separate subevent in the west with a progressive energy migration northward. The trend of this later subevent is subparallel to the northern fault plane selected by *Robinson* [2011]. The energy emission track lies in the neighborhood of a number of Robinson's relocated aftershocks and the estimated location of the large 1924 event [*Valenzuela and Wysession*, 1993]. The step of the energy emission to the west is a robust result unaffected by changes in the rate of expansion of the search grid or the nature of the time corrections made. No such displacement in the locus of the evocenter has been found in application of the same approach to great earthquakes in other environments [*Gorbatov et al.*, 2013], e.g., the M_w 8.1 2007 Solomons Islands event and the M_w 8.3 Sea of Okhotsk event for which we have close correspondence with backprojection from the USArray and European stations [*Ye et al.*, 2013] (see supporting information).

The dominant high-frequency emission for the 23 December 2004 lasts only about 60 s, which is quite short for such a large event. The long-period analysis of *Robinson* [2011] also indicates a comparable duration, rather shorter than the 100 s suggested by *Hayes et al.* [2009]. The long-period energy release appears to be largely confined to bilateral fracture along the curved fossil fracture zone 5 [*Mosher and Massell Symons*, 2008], yet we have additional high-frequency radiation to the west close to fracture zone 4. The presence of this second triggered subevent helps to reconcile the global centroid moment tensor results with those obtained just using the onset of the *P* waves.

4. Discussion and Conclusions

Recent large oceanic intraplate earthquakes have demonstrated complex behavior with rupture on multiple fault segments. The 1998 M_w 8.1 Antarctic Plate event produced a secondary area of rupture displaced well to the west of the initial rupture zone near the hypocenter, with a similar orientation [*Henry et al.*, 2000], though there may be low-level slip between the two patches [*Hjörleifsdóttir et al.*, 2009]. The M_w 8.6 and M_w 8.4 oceanic intraplate events on the Australian Plate south of Sumatra produced a complex pattern of faulting [*Yue et al.*, 2012; *Wang et al.*, 2012] with several segments apparently rupturing simultaneously.

In the 2004 event north of Macquarie Island, we seem to have a similar situation with subparallel faulting occurring simultaneously on relict structures from former fracture zones created when the Australian-Pacific Plate margin was divergent. Such multiple faulting may help to explain the relatively short duration of the event. The transition to oblique convergence with subduction of young crust is putting the Macquarie Block under significant strain that is eventually relieved by major failures reactivating the transform faults. The thin oceanic crust and relative strength of the oceanic mantle [e.g., *Kohlstedt et al.*, 1995] allow higher strain to be accumulated before failure than in continental environments, and we speculate that this favors stress transfer and triggering of secondary events once failure occurs in the largest events.

Spatial separation of high- and low-frequency components has recently been recognized as a common feature of megathrust events [*Lay et al.*, 2012; *Tajima et al.*, 2013]. Our results suggest that it may also play a role in other classes of great earthquakes.

Even for locations where the powerful techniques of backprojection from concentrated arrays [e.g., *Ishii et al.*, 2005; *Yue et al.*, 2012; *Wang and Mori*, 2011] cannot be brought to bear, it is possible to exploit the distributed global network to extract detailed information on the time evolution of the high-frequency emission from the source. By adopting a comparable approach to hypocenter determination, but now utilizing waveform segments rather than travel times, we can exploit strong spatial localization from good azimuthal control to characterize source behavior.

Acknowledgments

We thank the IRIS Data Management Centre for access to a broad range of seismic stations and data products. This paper is published with the permission of the Chief Executive Officer of Geoscience Australia.

The Editor thanks Rachel Abercrombie and an anonymous reviewer for their assistance in evaluating this paper.

References

Abercrombie, R., and G. Ekström (2001), Earthquake slip on oceanic transform faults, *Nature*, *410*, 74–77.

Bondar, I., and D. Storchak (2011), Improved location procedures at the International Seismological Centre, *Geophys. J. Int.*, *186*, 1220–1244.

Das, S. (1993), The Macquarie Ridge earthquake of 1989, *Geophys. J. Int.*, *115*, 778–798.

Engdahl, E. R., R. van der Hilst, and R. Buland (1998), Global teleseismic earthquake relocation with improved travel times and procedures for depth determination, *Bull. Seismol. Soc. Am.*, *88*, 722–743.

Gorbatov, A., S. Spiliopoulos, and B. L. N. Kennett (2013), Application of 3-D energy-projection for source properties of large events using small sets of well-distributed seismic stations, Abstract #1800540 presented at 2013 Fall Meeting, AGU, San Francisco, Calif.

Hayes, G. P., K. P. Furlong, and C. J. Ammon (2009), Intraplate deformation adjacent to the Macquarie Ridge south of New Zealand—The tectonic evolution of a complex plate boundary, *Tectonophysics*, *463*, 1–14.

Henry, C., S. Das, and J. H. Woodhouse (2000), The great March 25, 1998, Antarctic Plate earthquake: Moment tensor and rupture history, *J. Geophys. Res.*, *105*, 16,097–16,118.

Hjörleifsdóttir, V., H. Kanamori, and J. Tromp (2009), Modeling 3-D wave propagation and finite slip for the 1998 Balleny Islands earthquake, *J. Geophys. Res.*, *114*, B03301, doi:10.1029/2008JB005975.

Ishii, M., P. M. Shearer, H. Houston, and J. Vidale (2005), Extent, duration and speed of the 2004 Sumatra–Andaman earthquake imaged by the Hi-net array, *Nature*, *435*, 933–936.

Kennett, B. L. N., E. R. Engdahl, and R. Buland (1995), Constraints on seismic velocities in the Earth from traveltimes, *Geophys. J. Int.*, *122*, 108–124.

Kohlstedt, D. L., B. Evans, and S. J. Mackwell (1995), Strength of the lithosphere: Constraints imposed by laboratory experiments, *J. Geophys. Res.*, *100*, 17,587–17,602.

Lay, T., H. Kanamori, C. J. Ammon, K. D. Koper, A. R. Hutko, L. Ye, H. Yue, and T. M. Rushing (2012), Depth-varying rupture properties of subduction zone megathrust faults, *J. Geophys. Res.*, *117*, B04311, doi:10.1029/2011JB009133.

Mosher, S., and C. Massell Symons (2008), Ridge reorientation mechanisms: Macquarie Ridge Complex, Australia-Pacific plate boundary, *Geology*, *36*, 119–122.

Robinson, D. P. (2011), A rare great earthquake on an oceanic fossil fracture zone, *Geophys. J. Int.*, *186*, 1121–1134.

Ruff, L. J., J. W. Given, C. O. Sanders, and C. M. Sperber (1989), Large earthquakes in the Macquarie Ridge complex: Transitional tectonics and subduction initiation, *Pure Appl. Geophys.*, *129*, 71–129.

Simons, M., et al. (2011), The 2011 magnitude 9.0 Tohoku-Oki earthquake: Mosaicking the megathrust from seconds to centuries, *Science*, *332*, 1421–1425.

Tajima, F., J. Mori, and B. L. N. Kennett (2013), A review of the 2011 Tohoku-Oki earthquake (Mw 9.0): Large-scale rupture across heterogeneous plate coupling, *Tectonophysics*, *586*, 15–34.

Valenzuela, R. W., and E. M. Wysession (1993), Intraplate earthquakes in the southwest Pacific Ocean Basin and the seismotectonics of the southern Tasman Sea, *Geophys. Res. Lett.*, *20*, 2467–2470.

Walker, K. T., M. Ishii, and P. M. Shearer (2005), Rupture details of the 28 March 2005 Sumatra Mw 8.6 earthquake imaged with teleseismic *P* waves, *Geophys. Res. Lett.*, *32*, L24303, doi:10.1029/2005GL024395.

Walker, K. T., and P. M. Shearer (2009), Illuminating the near-sonic rupture velocities of the intracontinental Kokoxili Mw 7.8 and Denali fault Mw 7.9 strike-slip earthquakes with global P wave back projection imaging, *J. Geophys. Res.*, *114*, B02304, doi:10.1029/2008JB005738.

Wang, D., and J. Mori (2011), Rupture process of the 2011 off the Pacific coast of Tohoku earthquake (Mw 9.0) as imaged with back-projection of teleseismic P-waves, *Earth Planets Space*, *63*, 603–607.

Wang, D., J. Mori, and T. Uchide (2012), Supershear rupture on multiple faults for the Mw 8.6 Off Northern Sumatra, Indonesia earthquake of April 11, 2012, *Geophys. Res. Lett.*, *39*, L21307, doi:10.1029/2012GL053622.

Ye, L., T. Lay, H. Kanamori, and K. D. Koper (2013), Energy release of the 2013 Mw 8.3 Sea of Okhotsk earthquake and deep slab stress heterogeneity, *Science*, *341*, 1380–1384.

Yue, H., T. Lay, and K. D. Koper (2012), En échelon and orthogonal fault ruptures of the 11 April 2012 great intraplate earthquakes, *Nature*, *490*, 245–250.